Laboratory Investigation (2020) 100:712–726
https://doi.org/10.1038/s41374-019-0355-1

ARTICLE

Mitochondrial dysfunction/NLRP3 inflammasome axis contributes to angiotensin II-induced skeletal muscle wasting via PPAR-γ

Yuqing Liu[1] · Xiao Bi[1] · Yumei Zhang[1] · Yingdeng Wang[1] · Wei Ding[1]

Received: 30 March 2019 / Revised: 19 October 2019 / Accepted: 4 November 2019 / Published online: 19 December 2019

Abstract

Angiotensin II (Ang II) levels are elevated in patients with chronic kidney disease or heart failure, and directly causes skeletal muscle wasting in rodents, but the molecular mechanisms of Ang II-induced skeletal muscle wasting and its potential as a therapeutic target are unknown. We investigated the NLR family pyrin domain containing 3 (NLRP3) inflammasome-mediated muscle atrophy response to Ang II in C2C12 myotubes and *Nlrp3* knockout mice. We also assessed the mitochondrial dysfunction (MtD)/NLRP3 inflammasome axis in Ang II-induced C2C12 myotubes. Finally, we examined whether a peroxisome proliferator-activated receptor-γ (PPAR-γ) agonist could attenuate skeletal muscle wasting by targeting the MtD/NLRP3 inflammasome axis in vitro and in vivo. We demonstrated that Ang II increased NLRP3 inflammasome activation in cultured C2C12 myotubes dose dependently. *Nlrp3* knockdown or *Nlrp3*$^{-/-}$ mice were protected from the imbalance of protein synthesis and degradation. Exposure of C2C12 to Ang II increased mitochondrial ROS (mtROS) generation, accompanied by MtD. Remarkably, the mitochondrial-targeted antioxidant not only decreased mtROS and MtD, it also significantly inhibited NLRP3 inflammasome activation and restored skeletal muscle atrophy. Finally, the PPAR-γ agonist protected against Ang II-induced muscle wasting by preventing MtD, oxidative stress, and NLRP3 inflammasome activation in vitro and in vivo. This work suggests a potential role of MtD/NLRP3 inflammasome pathway in the pathogenesis of Ang II-induced skeletal muscle wasting, and targeting the PPAR-γ/MtD/NLRP3 inflammasome axis may provide a therapeutic approach for muscle wasting.

Introduction

Muscle wasting, characterized by loss of muscle mass, muscular weakness, and decreased force generation, is one of the most devastating clinical complications in chronic kidney disease (CKD), chronic heart failure (CHF), and cancer-associated cachexia, which leads to lower quality of life and increased morbidity and mortality [1]. Stimulation of the renin angiotensin system and increased levels of circulating angiotensin II (Ang II) are found in patients with CHF and CKD. Interestingly, increasing evidence indicates that Ang II, an endogenous peptide, plays a pivotal role in atrophic activity of skeletal muscle [2]. Enhanced protein proteolysis and reduced protein synthesis account for the onset of muscle wasting, which may be activated by effects of Ang II in a direct or indirect manner [3–6]. However, the understanding of explicit cellular mechanisms of Ang II in regulating the protein balance and as a potential therapeutic target remains unclear.

Many studies have indicated that inflammation is a crucial link in the onset of muscle wasting. Inflammatory cytokines including interleukin (IL)-6, tumor necrosis factor-α (TNF-α), and nuclear factor kappa B (NF-κB) act on the muscle protein imbalance via activating muscle proteolysis, paralleled by impairing muscle regeneration in many diseases [7]. However, limited benefits were observed in patients treated with IL-6 inhibitors or anti-TNFα therapy in clinical trials [8–10], which indicated that other inflammatory mediators might be involved in muscle wasting. The NLR family pyrin domain containing 3 (NLRP3) inflammasome may be implicated in skeletal muscle atrophy. Therefore, the potential role and mechanism of NLRP3 inflammasome in muscle wasting warrants further investigation.

These authors contributed equally: Yuqing Liu, Xiao Bi

✉ Wei Ding
gump1015@163.com

[1] Division of Nephrology, Shanghai Ninth People's Hospital, School of Medicine, Shanghai Jiaotong University, 639 zhizaoju Road, 200011 Shanghai, China

Oxidative stress generally refers to the elevated cellular production of reactive oxygen species (ROS), which function as signaling molecules that regulate the process of pathogen defense and programmed cell death [11]. The major sources of ROS generation in atrophic skeletal muscles depends on two oxidant systems, NADPH oxidase and the mitochondrial system [12]. Several studies have suggested that mitochondrial dysfunction (MtD) is involved in muscle wasting [13, 14]. Nevertheless, the relationship between mtROS/MtD and the NLRP3 inflammasome has not been discussed in skeletal muscle wasting.

PPAR-γ, one of the three different isoforms of peroxisome proliferator-activated receptors (PPARs), which are ligand-inducible transcription factors belonging to the family of nuclear hormone receptors, regulates adipogenesis, lipid biosynthesis, and energy balance [15]. PPAR-γ agonist exerts protective effects by preventing MtD in diverse pathological conditions, including diabetes [16], neurodegenerative diseases [17, 18], CKD, and cancer cachexia [19–21]. However, studies based on the protective response of PPAR-γ activation in skeletal muscle wasting are rare, especially those dealing with the induction of Ang II. Thus, in the present study, we explored the effects and underlying molecular mechanism of PPAR-γ activation on Ang II-induced skeletal muscle wasting.

Methods

Animal experiments

All animal procedures were approved by the Animal Care Committee at Shanghai Jiao Tong University. *Nlrp3*$^{-/-}$ mice on a C57BL/6J background (Jackson Laboratory, Sacramento, CA, USA) were used to detect the role of NLRP3 inflammasome activation in Ang II-induced muscle wasting. Heterozygous littermates were bred to generate homozygous knockout (KO) mice and littermates wild-type (WT) controls. Mice were maintained in a temperature-controlled environment with a 12-h light/dark cycle and fed a routine rodent diet. The animal model of muscle wasting was created by implanting an osmotic mini-pump to infuse Ang II (AngII 500 ng/kg/min subcutaneously, $n = 6$) or saline ($n = 6$) for 4 weeks. In the Ang II + Rosi group or Rosi group, mice were treated with rosiglitazone (Rosi) (10 mg/kg/day, intragastric administration, $n = 6$) for 4 weeks.

Cell culture and differentiation

Mouse C2C12 myoblasts were purchased from the ATCC (Manassas, VA, USA) and cultured in high glucose Dulbecco's modified Eagle's medium (DMEM) supplemented with 10% fetal bovine serum (FBS). To initiate cell differentiation at a confluence of 80–90%, we allowed the cells to reach 100% confluence, changed the medium to high glucose DMEM containing 2% horse serum, and replaced the medium every 2 days. After 4–5 days of differentiation, the C2C12 myotubes were used for the subsequent experiments.

Transfection of short interfering RNAs

On day 4 after C2C12 myotube differentiation, the media of the C2C12 cells were replaced with siRNA transfection medium. The cells were then transfected with NLRP3 short interfering RNA (siRNA) (siNLRP3) (100 nmol/L) or control siRNA (siNC) (100 nmol/L) using Lipofectamine 3000 (Invitrogen) according to the manufacturer's protocols. After 24 h of transfection with the siRNAs, C2C12 myotubes were used for subsequent experiments. The depletion of NLRP3 was confirmed by western blotting.

Mitochondrial membrane potential (△ψm) assessment

To evaluate mitochondrial function, we employed JC-1 staining to quantitatively determine alterations of △ψm. Briefly, C2C12 myotubes were cultured in a 6-well plate with the indicated treatment. The cells were then washed with ice-cold phosphate-buffered saline (PBS), incubated with JC-1 for 20 min at 37 °C and washed twice with ice-cold PBS. The myotubes were then visualized under a fluorescent microscope at an excitation wavelength of 488 nm and emission wavelengths of 530 nm (green) and 590 nm (red). JC-1 aggregates are presented as red fluorescence while JC-1 monomers show green fluorescence. Thus, the alterations of △ψm could be measured as the ratio of red/green fluorescence intensities. The red or green fluorescence intensity was quantified by Image-pro plus 6.0 and the results were expressed as the fluorescence intensity ratio of red to green normalized with the control group.

MitoSOX and 2′,7′-dichlorofluorescin diacetate staining

Mitochondrial superoxide is detected by MitoSOX staining, and intracellular ROS is detected using 2′,7′-dichlorofluorescin diacetate (DCFDA) staining, according to the manufacturer's instructions (Invitrogen, USA). Briefly, C2C12 myotubes with corresponding treatment were incubated with the MitoSOX working solution for 30 min at 37 °C. The myotubes were then washed with PBS gently and observed under a Nikon fluorescent microscope. To detect intracellular ROS, 2′,7′-dichlorodihydrofluorescein diacetate (DCFH-DA) was dissolved in dimethyl sulfoxide (DMSO) and diluted to 10 μM with serum-free media. After 48 h of treatment, C2C12

myotubes were washed with PBS and incubated with DCFDA for 30 min at 37 °C. The myotubes were then visualized under a fluorescent microscope. The results were presented as the average fluorescence intensity normalized with the control group.

Superoxide dismutase 2, malondialdehyde measurement, and ATP assay

The superoxide dismutase 2 (SOD2) activity and malondialdehyde (MDA) level in the gastrocnemius muscle were measured using a colorimetric assay kit (Beyotime Institute of Biotechnology) following the manufacture's protocol. The absorbance of the samples was detected using a microplate reader at 450 nm (SOD2) and 533 nm (MDA). All results were expressed as U/mg protein and nmol/mg protein, respectively. The ATP content in gastrocnemius muscle tissues was measured using an ATP assay kit (Beyotime Institute of Biotechnology) according to the manufacturer's protocol.

Western blotting and antibodies

C2C12 cells and gastrocnemius muscle tissues were collected and lysed in lysis buffer for protein extraction. Equal amounts of proteins were then resolved electrophorectically and transferred to polyvinylidene fluoride (PVDF) membranes. The membranes were blocked with 5% nonfat milk for 1 h and then incubated with primary antibody overnight at 4 °C. The membranes were then incubated with secondary antibodies and visualized using an enhanced chemiluminescent system (Amersham, UK). The intensities of the immunoreactive proteins were quantified using Image J and normalized to the intensity of β-actin. The primary antibodies were used as follows: anti-MyHC (myosin heavy chain; R&D Systems, USA), anti-PPAR-γ (Cell Signaling Technology, USA), anti-NLRP3 (Life Science, USA), anti-ASC (apoptosis-associated speck-like protein containing a CARD; Life Science, USA), anti-IL-18 (MBL, USA), anti-IL-1β (R&D Systems, USA), anti-caspase-1 (Santa Cruz, USA), anti-Akt (Santa Cruz, USA), anti-p-Akt (Santa Cruz, USA), anti-PI3K (Santa Cruz, USA), anti-p-PI3K (Santa Cruz, USA), anti-mTOR (Santa Cruz, USA), anti-p-mTOR (Santa Cruz, USA), and anti-β-actin (Millipore, USA).

RNA extraction and quantitative RT-PCR

C2C12 cells and gastrocnemius muscle tissue were homogenized in the TRizol reagent (Thermo Scientific, Wilmington, MA, USA) to extract total RNA, following the manufacture's protocol. First-strand cDNA was reverse transcribed from total RNA using the RT reagent kits, according to the manufacture's recommendations. Real-time PCR was then conducted using a SYBR Green Master Mix on the ABI Prism 7500 Sequence Detection System (Foster City, CA, USA). The relative expression was quantified using the comparative $2^{-\Delta\Delta Ct}$ method and normalized against the expression of *Gapdh*. The sequence-specific primers used for PCR amplification are shown in Table 1.

Grip strength

The forelimb grip strength of the mice was measured by grip strength measurement (Life Science, USA) according to previously published methods [22]. Mice were permitted to grasp the bar mounted on the force gauge. The gauge was reset to 0 g after stabilization, and the mouse were pulled by the tail until they let go of the bar. During this process, the peak pull force was recorded on a digital force transducer. Each mouse went through five consecutive force measurements, with 1-min interval between tests. The five records for each mouse were averaged for statistical analysis.

Transmission electron microscopy

A portion of the gastrocnemius muscle samples was fixed in 2.5% glutaraldehyde in phosphate buffer at room temperature. Subsequently, the samples were rinsed with 1 mmol/L phosphoric acid solution, post-fixed in 1% osmium tetroxide, and embedded in Epon resin. Ultrathin sections (60 nm) were prepared and place on copper grids, and then stained with uranyl acetate and lead citrate for observation using a transmission electron microscopy.

Immunofluorescence staining and myofiber size measurement

Gastrocnemius muscles were snap-frozen in isopentane cooled by liquid nitrogen and cut into 10-μm sections. The slices were fixed with acetone, washed with PBS, and blocked by 1% bovine serum albumin for 20 min. The sections were then incubated with anti-dystrophin primary antibodies at 4 °C overnight and with the secondary antibody for 30 min in the dark at room temperature. Images were captured under a Nikon fluorescent microscope to evaluate myofiber cross-sectional areas using the ImageJ software. At least 300 myofibers in each mouse gastrocnemius muscle were examined.

Statistical analysis

All results were expressed as the mean ± standard deviation (mean ± SD) unless otherwise stated. Data were analyzed with one-way analysis of variance (ANOVA) followed by

Table 1 Primer sequences used in the present study.

Gene	Forward primer	Reverse primer
Atrogin-1 (*Fbxo32*)	CAGCTTCGTGAGCGACCTC	GGCAGTCGAGAAGTCCAGTC
MuRF-1 (*Trim63*)	GTGTGAGGTGCCTACTTGCTC	GCTCAGTCTTCTGTCCTTGG
myostatin (Mstn)	AGTGGATCTAAATGAGGGCA	GGTTTCCAGGCGCAGCTTAC
mtDNA	TTTTATCTGCATCTGAGTTTAA	CCACTTCATCTTACCATTTAT
Mt-nd1	ATCCTCCCAGGATTTGGAAT	ACCGGTAGGAATTGCGATAA
Gapdh	AGGTCGGTGTGAACGGATTTG	TGTAGACCATGTAGTTGAGG

MuRF-1 muscle-specific RING finger protein 1 (also known as tripartite motif containing 63 (Trim63)), *mtDNA* mitochondrial DNA, *MT-ND1* mitochondrially encoded NADH:ubiquinone oxidoreductase core subunit 1, *GAPDH* glyceraldehyde-3-phosphate dehydrogenase

Tukey's post hoc test using SPSS 20.0. In all cases, $p < 0.05$ was considered statistically significant.

Results

NLRP3 inflammasome activation leads to Ang II-induced muscle wasting in vitro

To investigate the role of Ang II in NLRP3 inflammasome activation, we stimulated C2C12 myotubes with different doses (10^{-8}, 10^{-7}, 10^{-6}, and 10^{-5} mol/L) of Ang II. As shown in Fig. 1a, b, Ang II directly activated the NLRP3 inflammasome by the induction of NLRP3 protein and its downstream components ASC, caspase-1, IL-1β, and IL-18 in a dose-dependent manner. Many studies have proved that Ang II-induced muscle wasting [2]. Inhibition of *Nlrp3* via siRNA treatment reduced the level of the NLRP3 protein significantly (Fig. 1c) and the Ang II-induced reduction of MyHC protein level was remarkably attenuated (Fig. 1d, e). Moreover, the PI3K/AKT/mTOR signaling pathway was inhibited by Ang II stimulation (10^{-6} mol/L) presented by the decreased protein levels of phosphorylated PI3K, phosphorylated Akt, and phosphorylated mTOR (Fig. 1d, e). Accordingly, the mRNA level of muscle proteolytic genes Atrogin-1, MuRF-1, and myostatin were increased in the Ang II group (Fig. 1f). However, the Ang II-induced muscle wasting was rescued by treatment with siNLRP3, which indicated that *Nlrp3* silencing significantly attenuated the Ang II-induced protein imbalance.

Nlrp3$^{-/-}$ mice attenuate Ang II-induced muscle wasting in vivo

To further confirm the effects of Ang II on NLRP3 inflammasome activation, the expressions of NLRP3 inflammasome-associated proteins were observed in WT mice with the infusion of Ang II using a micro-osmotic pump at different times (0, 1, 2, 3, 4 weeks). As shown in Fig. 2a, b, Ang II directly activated the NLRP3 inflammasome by the induction of NLRP3 protein and its downstream components ASC, caspase-1, IL-1β, and IL-18 in a time-dependent manner. To evaluate whether NLRP3 deficiency exerted an ameliorative effect on muscle wasting, we examined WT and *Nlrp3*$^{-/-}$ mice after the infusion of Ang II using a micro-osmotic pump for 4 weeks. As shown in Fig. 2d, e, the WT mice treated with Ang II manifested progressive body weight loss (Fig. 2d) and reduced gastrocnemius muscle mass (normalized to tibia length; Fig. 2e), which was reversed by NLRP3 deficiency. Improved muscle function, as assessed by grip strength, was also observed in *Nlrp3*$^{-/-}$ mice treated with Ang II (Fig. 2f). In addition, as shown in Fig. 2g–j, compared with the WT mice treated with Ang II, the *Nlrp3*$^{-/-}$ mice treated with Ang II exhibited remarkably increased muscle mass, characterized by increased mean myofiber area (Fig. 2g, j) and a rightward shift in the distribution of myofiber size area (Fig. 2i), which was in consistent with above improvement in muscle function. At the molecular level, depletion of NLRP3 improved the muscle wasting characterized by increased MyHC protein level, increased protein expressions of phosphorylated PI3K (p-PI3K), phosphorylated Akt (p-Akt), and phosphorylated mTOR (p-mTOR), as well as decreased mRNA expressions of muscle proteolytic genes Atrogin-1, MuRF-1, and Myostatin (Fig. 2k–m).

The mtROS/MtD/NLRP3 inflammasome axis induces Ang II-induced muscle wasting in C2C12 myotubes

To identify whether mitochondrial ROS (mtROS) and MtD occupy an important position in Ang II-induced muscle wasting, C2C12 myotubes were pretreated with Mito-TEMPO (10 μM) for 1 h and then incubated with Ang II (10^{-6} mol/L).

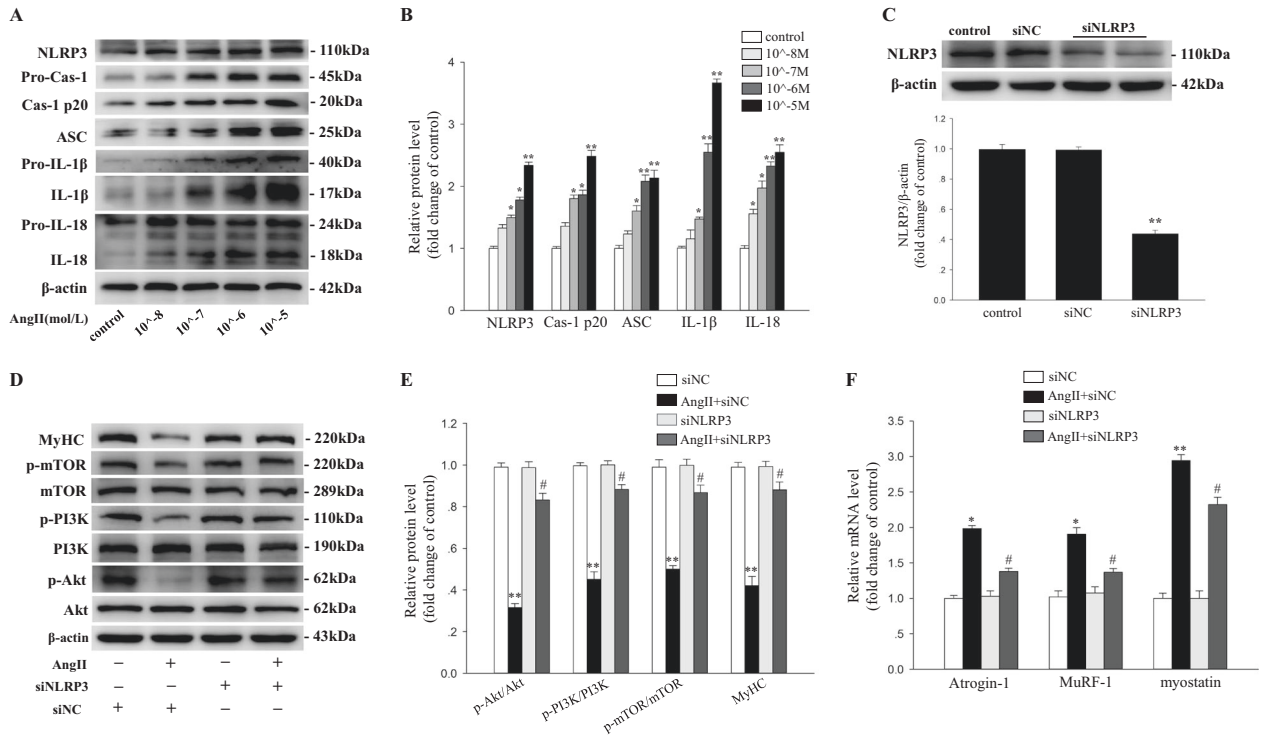

Fig. 1 NLRP3 inflammasome activation contributes to Ang II-induced muscle wasting in vitro. a Protein expression of NLRP3, caspase-1, ASC, IL-1β, and IL-18 in C2C12 myotubes after stimulation by Ang II in different doses (10^{-8}, 10^{-7}, 10^{-6}, and 10^{-5} mol/L) was detected by western blotting. **b** Quantification of NLRP3, caspase-1, ASC, IL-1β, and IL-18 expression normalized to β-actin. **c** Protein expression of NLRP3 in C2C12 myotubes treated with siNLRP3 or siNC and quantification of NLRP3 expression normalized to β-actin. **d** Protein expressions of MyHC, p-Akt, Akt, p-PI3K, PI3K, p-mTOR, and mTOR in C2C12 myotubes transfected with siNLRP3 or siNC with or without Ang II were detected by western blot. **e** Quantification of MyHC, the ratio of p-Akt to Akt, p-PI3K to PI3K, p-mTOR to mTOR expression normalized to β-actin. **f** The mRNA expression of muscle proteolytic genes including Atrogin-1, MuRF-1, and myostatin in C2C12 myotubes transfected with siNLRP3 or siNC with or without Ang II normalized to *Gapdh* was performed using real-time PCR. Data represent the mean ± SD ($n = 6$). $^{*}P < 0.05$, compared with the control group or siNC group, $^{**}P < 0.01$, compared with the control group or siNC group. $^{\#}P < 0.05$, the Ang II + siNLRP3 group versus the Ang II + siNC group. siNC: control siRNA, siNLRP3: NLRP3 siRNA.

The results showed that Mito-TEMPO treatment induced an elevated MyHC protein level and increased expressions of p-PI3K, p-Akt, and p-mTOR, accompanied by decreased expression of muscle proteolytic genes Atrogin-1, MuRF-1, and myostatin (Fig. 3a–c). Meanwhile, increased oxidative stress was observed in the Ang II group, including decreased SOD2 activity and elevated MDA levels (Fig. 3d, e). Additionally, after treatment with Ang II, we found that Ang II induced increased total ROS production and mitochondrial ROS, characterized by elevated fluorescent intensity of DCF and MitoSOX (Fig. 3f, g). In addition, as shown in Fig. 3h–l, Ang II induced MtD, characterized by impaired mitochondrial membrane potential (△ψm), decreased mtDNA copy numbers, decreased the mitochondrially encoded NADH:ubiquinone oxidoreductase core subunit 1 (MT-ND1) level, and reduced ATP content. By contrast, these effects were significantly reversed by Mito-TEMPO treatment. Taken together, these results indicated that mtROS and MtD are involved in Ang II-induced muscle wasting in C2C12 myotubes.

To further explore the relationship between mtROS/MtD and NLRP3 inflammasome activation in response to Ang II-induced muscle wasting, we hypothesized that the MtD/NLRP3 inflammasome axis mediated AngII-induced muscle wasting. Therefore, we detected the effect of Mito-TEMPO (MT) on NLRP3 inflammasome activation induced by Ang II in C2C12 myotubes. As expected, compared with the Ang II group, the protein levels of NLRP3, ASC, caspase-1, IL-1β, and IL-18 were downregulated in the Ang II + MT group (Fig. 3m, n). Thus, we concluded that the mtROS/MtD/NLRP3 inflammasome axis is involved in Ang II-induced muscle wasting in C2C12 myotubes.

PPAR-γ agonist attenuates muscle wasting by inhibiting mtROS/MtD and NLRP3 inflammasome activation in C2C12 myotubes

To further investigate the mechanism of Ang II-induced muscle wasting, we examined the role of PPAR-γ in Ang II-induced muscle wasting, MtD, and NLRP3 inflammasome activation. In vitro, C2C12 myotubes were incubated with Ang II (10^{-6} mol/L) following pretreatment with the PPAR-γ agonist rosiglitazone (10 μM) for 1 h.

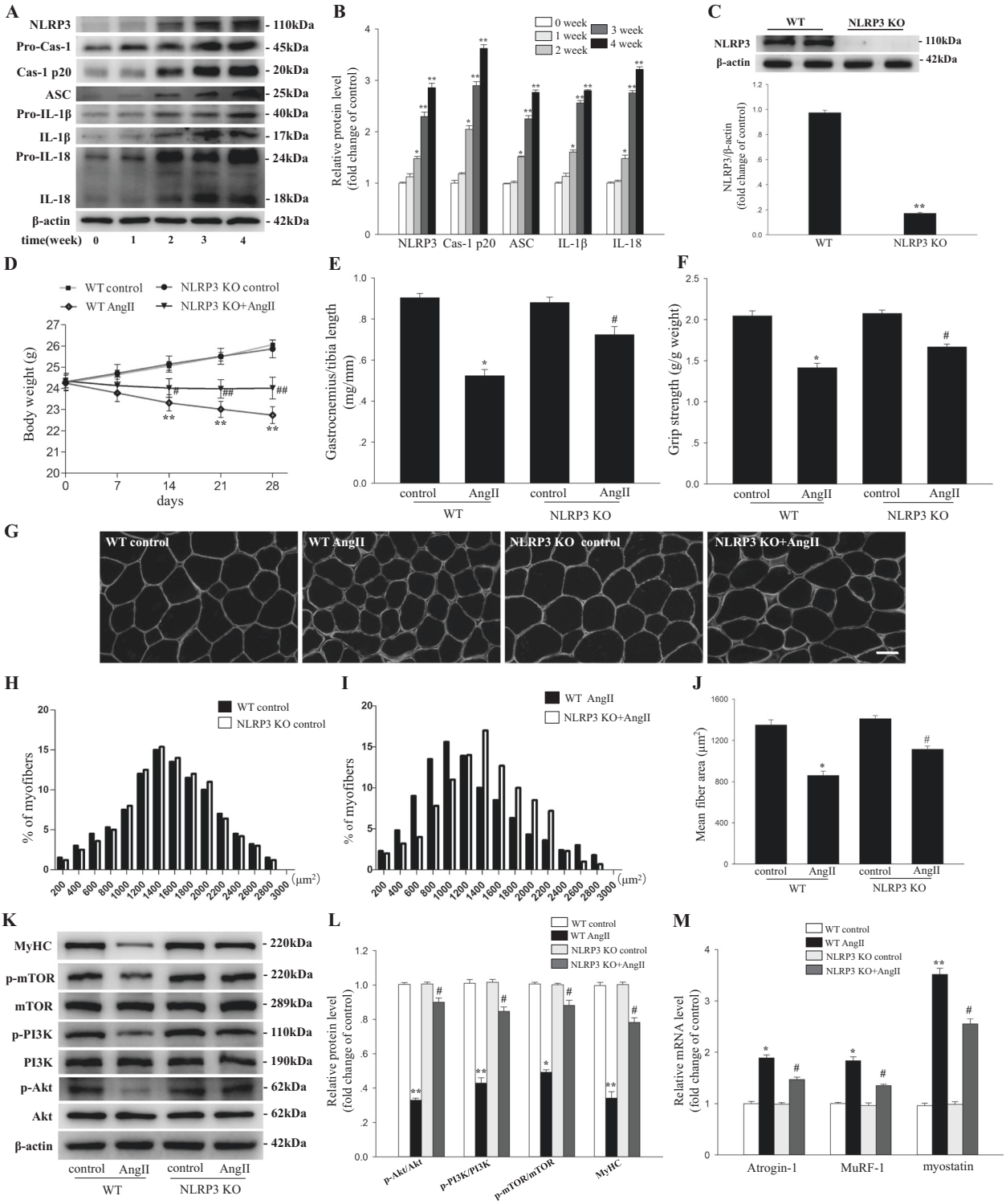

As shown in Fig. 4a–c, the disruption of protein synthesis (such as p-PI3K, p-Akt, and p-mTOR protein) and the induction of protein degradation (such as Atrogin-1, MuRF-1, and myostatin) were reversed by rosiglitazone treatment. In addition, the Ang II-induced increase in cellular ROS and mtROS (Fig. 4f, g), manifested by increased fluorescent intensity of DCF and MitoSOX, respectively, as well as the elevated level of oxidative stress, represented by reduced SOD2 activity (Fig. 4d) and increased MDA levels (Fig. 4e), were attenuated by rosiglitazone treatment. Unsurprisingly, as shown in Fig. 4h–l, rosiglitazone ameliorated MtD characterized by impaired mitochondrial

◀ **Fig. 2 *Nlrp3*$^{-/-}$ mice ameliorated Ang II-induced muscle wasting in vivo. a** Protein expressions of NLRP3, caspase-1, ASC, IL-1β, and IL-18 in wild-type (WT) mice with the infusion of Ang II using a micro-osmotic pump at different times (0, 1, 2, 3, 4 weeks) were detected by western blotting. **b** Quantification of NLRP3, caspase-1, ASC, IL-1β, and IL-18 expression normalized to β-actin. **c** Western blot analysis of NLRP3 protein level in WT mice and *Nlrp3*$^{-/-}$ mice, and quantification of NLRP3 expression normalized to β-actin. **d** Body weight changes in the WT mice and *Nlrp3*$^{-/-}$ mice with or without Ang II. **e** Gastrocnemius muscle weight normalized to tibia length. **f** Assessment of muscle grip strength in the WT mice and *Nlrp3*$^{-/-}$ mice with or without Ang II. **g** Representative micrographs of gastrocnemius sections with dystrophin staining (scale bar: 20 μm, magnification: 400×). **h** & **i** Distribution of myofiber cross-sectional area (CSA) in gastrocnemius muscles of the WT mice and *Nlrp3*$^{-/-}$ mice with or without Ang II. **j** Mean myofiber area in gastrocnemius muscles. **k** Protein expression of MyHC, p-Akt, Akt, p-PI3K, PI3K, p-mTOR, and mTOR in gastrocnemius muscles was determined by western blotting. **l** Quantification of MyHC, the ratio of p-Akt to the Akt, p-PI3K to PI3K, and p-mTOR to mTOR expression normalized to β-actin. **m** The mRNA expression of Atrogin-1, MuRF-1, and myostatin in gastrocnemius muscles of the WT mice and *Nlrp3*$^{-/-}$ mice with or without Ang II normalized to *Gapdh*. Data represent the mean ± SD ($n = 6$). *$P < 0.05$, compared with the WT control group, **$P < 0.01$, compared with the WT control group. $^{\#}P < 0.05$, the *Nlrp3*$^{-/-}$/Ang II group versus the WT/Ang II group.

membrane potential (△ψm), and decreased mtDNA copy numbers, the MT-ND1 level, and the ATP content. Furthermore, as shown by western blotting analysis, upregulation of the protein levels of NLRP3, ASC, caspase-1, IL-1β, and IL-18 by Ang II stimulation was suppressed by rosiglitazone treatment (Fig. 4m, n).

PPAR-γ antagonist aggravates muscle wasting by increasing mtROS/MtD and NLRP3 inflammasome activation in C2C12 myotubes

To further confirm the possible underlying mechanism, PPAR-γ antagonist T0070907 (10 μM) was used to validate whether PPAR-γ could serves as a regulator of the MtD/NLRP3 inflammasome axis in Ang II-induced muscle wasting. Decreased protein expressions of MHC, p-PI3K, p-Akt, and p-mTOR as well as increased expression of muscle proteolytic genes (Atrogin-1, MuRF-1, and myostatin) in the Ang II group were exacerbated by treatment with the PPAR-γ antagonist T0070907 in C2C12 myotubes (Fig. 5a–c). Additionally, the increased oxidative stress presented by reduced SOD2 activity (Fig. 5d) and elevated MDA level (Fig. 5e) as well as the increased cellular ROS and mtROS generation shown by DCFDA staining and MitoSOX staining, respectively (Fig. 5f, g), in the Ang II group were exacerbated by T0070907 treatment in C2C12 myotubes. Accordingly, decreased △ψm, mtDNA copy numbers, the MT-ND1 level, and ATP content induced by Ang II treatment were also aggravated in the AngII + T007097 group (Fig. 5h–l). Besides, NLRP3 inflammasome activation, represented by upregulated protein levels of NLRP3, ASC, caspase-1, IL-1β, and IL-18, was also exacerbated by T0070907 treatment in C2C12 myotubes (Fig. 5m, n).

PPAR-γ agonist rosiglitazone ameliorates Ang II-induced muscle wasting in vivo

To confirm the role of PPAR-γ in Ang II-induced muscle wasting, we established an animal model by infusion of Ang II using a micro-osmotic pump in WT mice. The Ang II group showed progressive body weight loss (Fig. 6a) and decreased gastrocnemius muscle mass normalized to tibia lengths (Fig. 6b), accompanied by impaired muscle function as assessed by grip strength (Fig. 6c), which were remarkably restored by rosiglitazone treatment. As shown in Fig. 6d–g, in accordance with improved muscle function, the Ang II mice treated with rosiglitazone showed increased muscle mass, represented by increased mean myofiber area and a rightward shift in the distribution of myofiber sizes area. Accordingly, the protein imbalance, characterized by decreased protein synthesis (such as MyHC, p-PI3K, p-Akt, and p-mTOR) and increased protein degradation (such as Atrogin-1, MuRF-1 and myostatin), was reversed by rosiglitazone administration by virtue of increasing PPAR-γ activity (Fig. 6h–j).

PPAR-γ agonist rosiglitazone attenuates muscle wasting by preventing MtD and NLRP3 inflammasome activation in vivo

To further determine whether PPAR-γ/MtD/NLRP3 inflammasome signaling exerts a vital role in Ang II-induced muscle wasting, oxidative stress, MtD, and NLRP3 inflammasome activation were assessed in vivo. As shown in Fig. 7a, b, enhanced SOD2 activity and decreased MDA level were detected in gastrocnemius muscles of the Ang II mice treated with rosiglitazone. Additionally, abnormal mitochondria, characterized by swelling with vacuolar degeneration and fragmented cristae, were observed by TEM in the Ang II group, which was reversed by rosiglitazone treatment (Fig. 7c). Accordingly, increased ATP levels, mtDNA, and *Mt-nd1* mRNA expression were also observed in the Ang II mice treated with rosiglitazone (Fig. 7d–f). Moreover, rosiglitazone administration also decreased NLRP3 inflammasome activation, represented by reduced NLRP3, ASC, caspase-1, IL-1β, and IL-18 protein levels (Fig. 7g, h).

Discussion

Overactivation of the renin-angiotensin system (RAS), especially Ang II, plays a central role in the pathogenesis and progression of various chronic diseases. The aim of this study was to determine the exact molecular mechanisms of

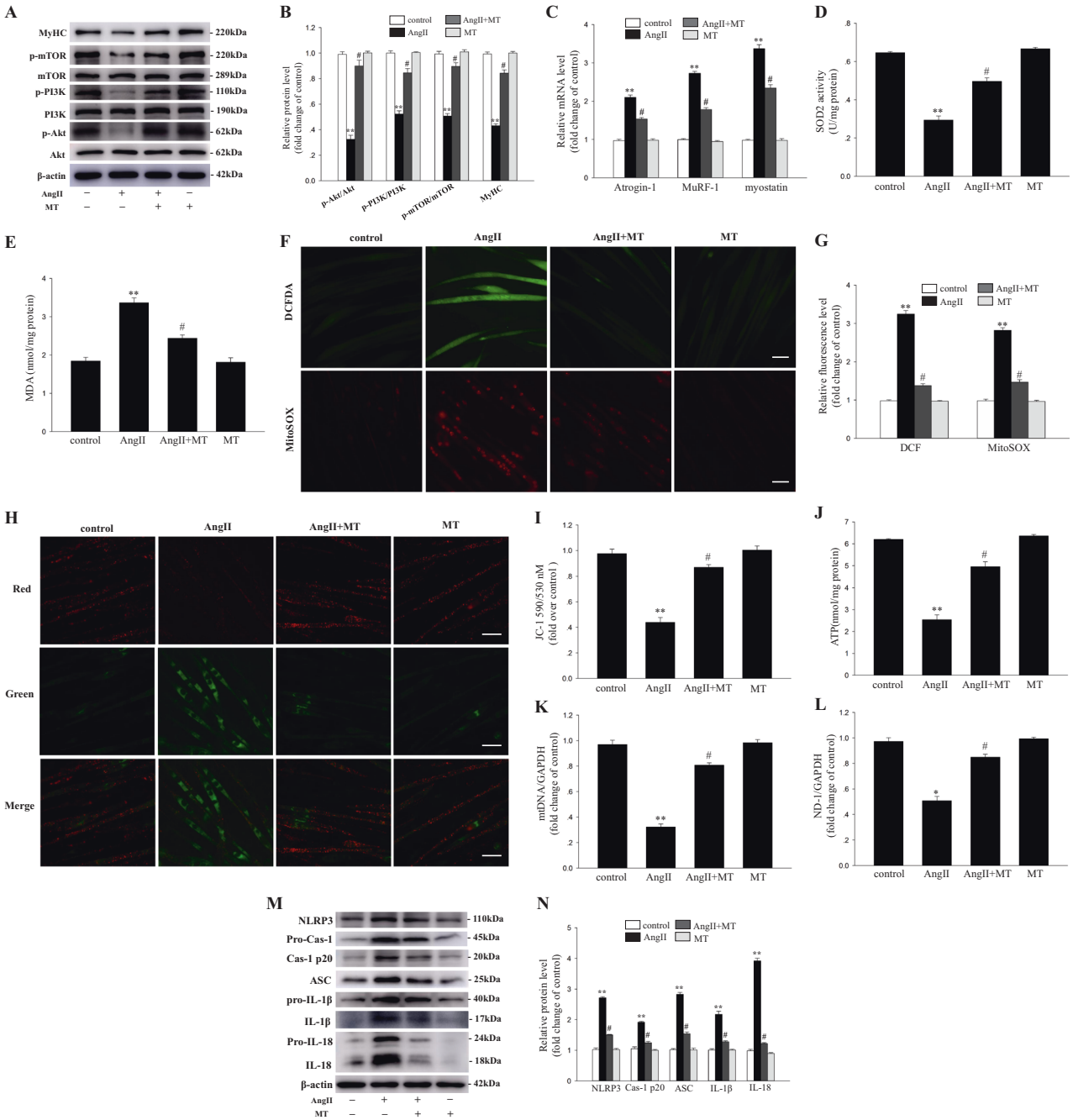

Fig. 3 The mtROS/MtD/NLRP3 inflammasome axis is involved in Ang II-induced muscle wasting in C2C12 myotubes. Cells were pretreated with Mito-TEMPO (10 μM) for 1 h and then incubated with Ang II (10^{-6} mol/L) for 24 h. **a** Western blotting analysis of MyHC, p-Akt, Akt, p-PI3K, PI3K, p-mTOR, and mTOR in gastrocnemius muscles. **b** Quantification of MyHC, the ratio of p-Akt to the Akt, p-PI3K to PI3K, p-mTOR to mTOR expression normalized to β-actin. **c** The mRNA level of *Fbxo32* (Atrogin-1), *Trim63* (MuRF-1), and *Mstn* (myostatin) in C2C12 myotubes normalized to *Gapdh* was performed using real-time PCR. **d** & **e** The SOD2 activity and MDA level in C2C12 myotubes were determined according to the manufacturer's protocols. **f** Representative images of total ROS production stained with dichlorodihydrofluorescein diacetate (DCFDA) (10 μM) and mitochondrial ROS stained with MitoSOX Red (5 μM) in C2C12 myotubes, respectively (scale bar: 50 μm, magnification: 200×). **g** Quantification of 2′,7′-dichlorofluorescein and MitoSOX Red fluorescence intensity, respectively. **h** Representative images of JC-1 staining in C2C12 myotubes. JC-1 aggregates (590 nm, red); JC-1 monomers (530 nm, green) (scale bar: 50 μm, magnification: 200×). **i** Quantification of JC-1 fluorescence intensity. **j** ATP production in C2C12 myotubes was determined according to the manufacturer's protocol. **k**, **l** The mtDNA copy number and *Mt-nd1* level in C2C12 myotubes normalized to *Gapdh* were detected using real-time PCR, respectively. **m** Western blotting analysis of NLRP3, caspase-1, ASC, IL-1β, and IL-18 in C2C12 myotubes. **n** Quantification of NLRP3, caspase-1, ASC, IL-1β, and IL-18 expression normalized to β-actin. The values represent the mean ± SD ($n = 6$). *$P < 0.05$, compared with the control group, **$P < 0.01$, compared with the control group. #$P < 0.05$, the Ang II + MT group versus the Ang II group. MT, Mito-TEMPO.

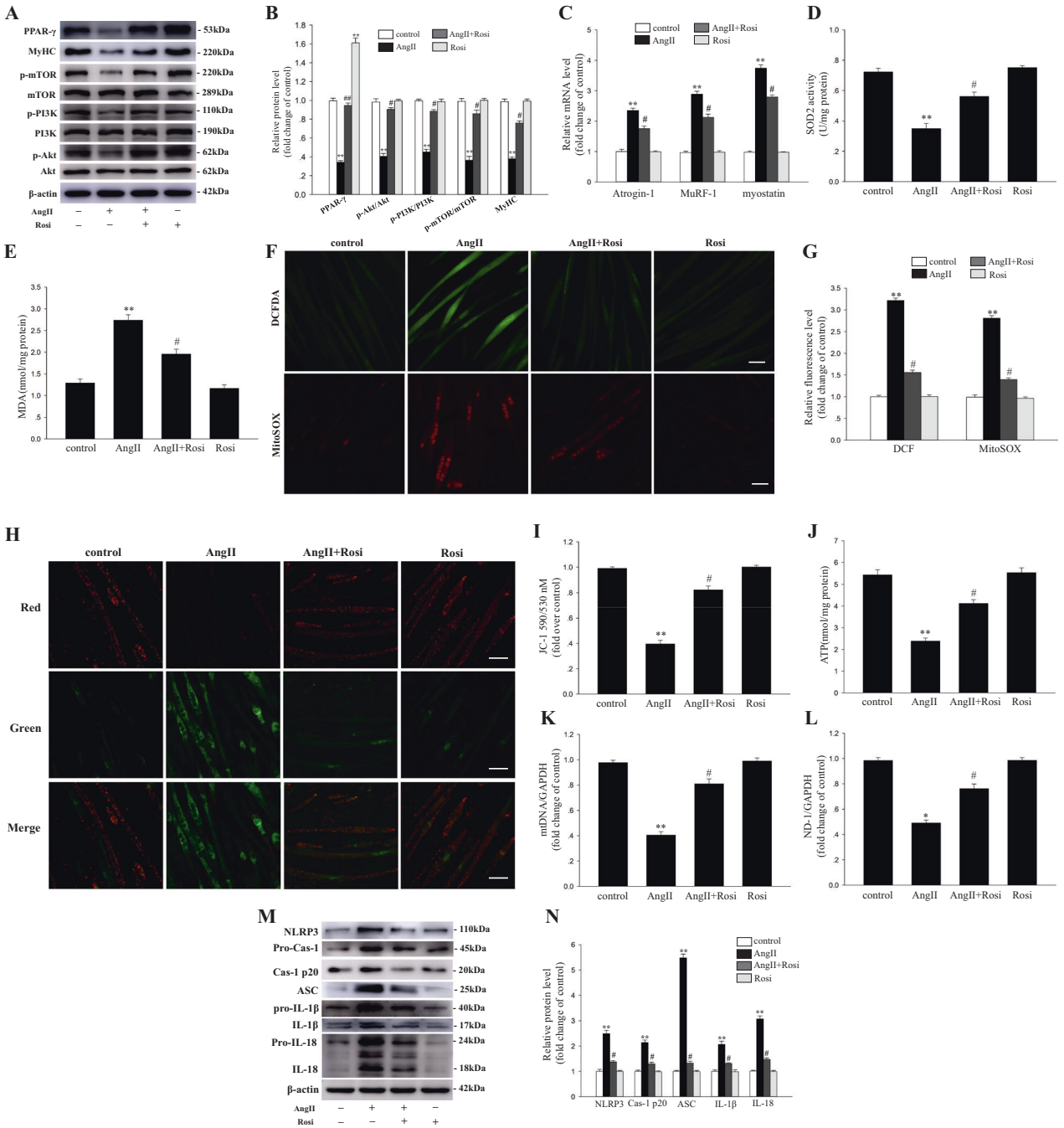

Fig. 4 The PPAR-γ agonist rosiglitazone attenuated Ang II-induced muscle wasting by inhibiting mtROS/MtD and NLRP3 inflammasome activation in C2C12 myotubes. Cells were pretreated with rosiglitazone (10 μM) for 1 h and then incubated with Ang II (10^{-6} mol/L) for 24 h. **a** Western blotting analysis of PPAR-γ, MyHC, p-Akt, Akt, p-PI3K, PI3K, p-mTOR, and mTOR in C2C12 myotubes. **b** Quantification of PPAR-γ, MyHC, the ratio of p-Akt to the Akt, p-PI3K to PI3K, and p-mTOR to mTOR expression normalized to β-actin. **c** The mRNA level of Atrogin-1, MuRF-1, and myostatin in C2C12 myotubes was performed using real-time PCR. **d** & **e** The SOD2 activity and MDA level in C2C12 myotubes were determined according to the manufacturer's protocol. **f** Representative images of total ROS production by DCFDA staining and mitochondrial ROS by MitoSOX Red staining in C2C12 myotubes (scale bar: 50 μm, magnification: 200×). **g** Quantification of 2′,7′-dichlorofluorescein and MitoSOX Red fluorescence intensity. **h** Representative images of JC-1 staining in C2C12 myotubes. JC-1 aggregates (590 nm, red); JC-1 monomers (530 nm, green) (scale bar: 50 μm, magnification: 200×). **i** Quantification of JC-1 fluorescence intensity. **j** ATP production in C2C12 myotubes was determined according to the manufacturer's protocol. **k**, **l** The mtDNA copy number and *Mt-ND1* level in C2C12 myotubes normalized to *Gapdh* were detected using real-time PCR. **m** Western blotting analysis of NLRP3, caspase-1, ASC, IL-1β, and IL-18 in C2C12 myotubes. **n** Quantification of NLRP3, caspase-1, ASC, IL-1β, and IL-18 expression normalized to β-actin. The values represent the mean ± SD ($n = 6$). $^{*}P < 0.05$, compared with the control group; $^{**}P < 0.01$, compared with the control group. $^{\#}P < 0.05$, the Ang II + Rosi group versus the Ang II group. Rosi, rosiglitazone.

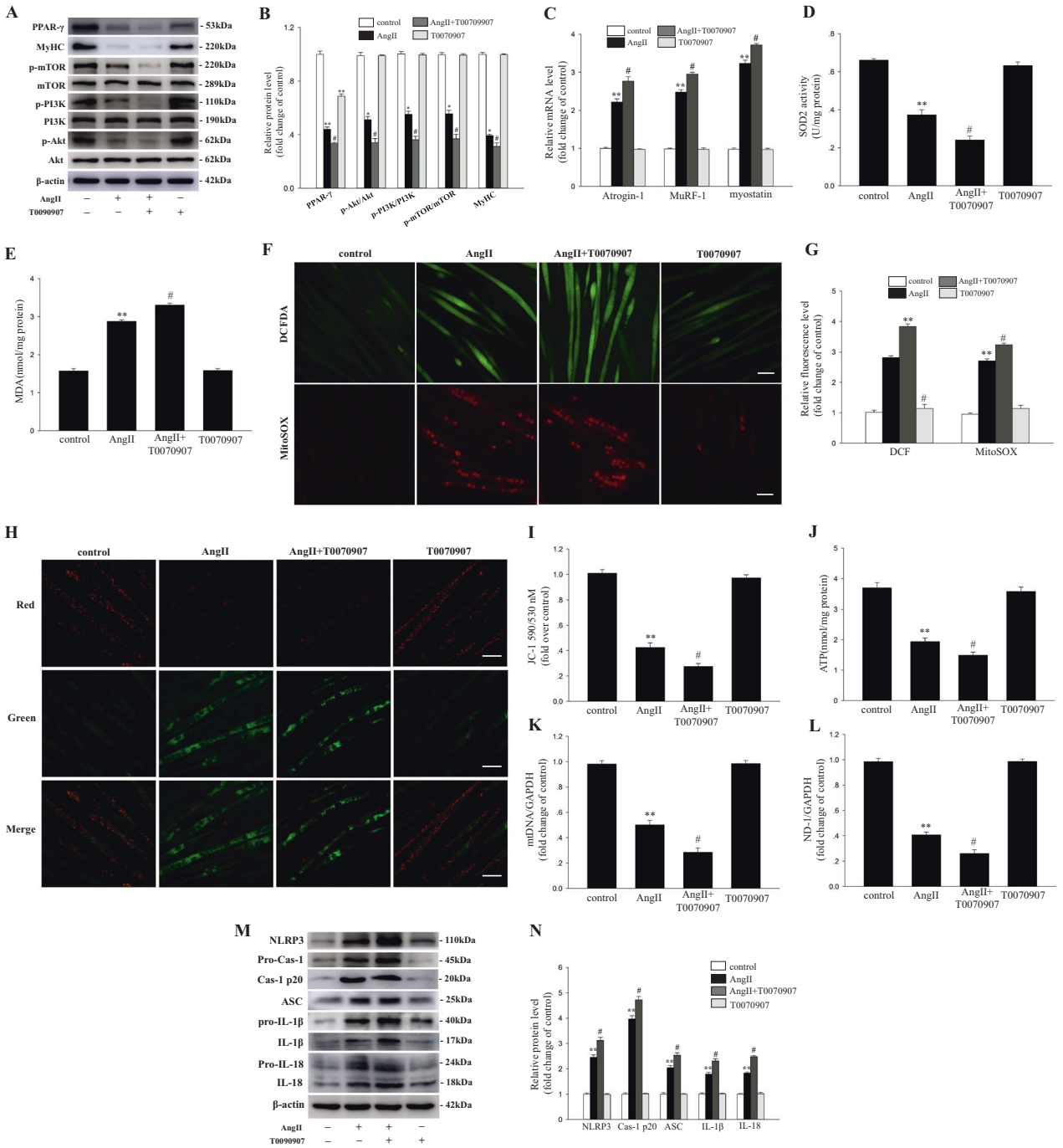

Ang II-induced muscle wasting. The results revealed that NLRP3 inflammasome activation contributes to Ang II-induced muscle wasting. Ang II dose-dependently triggered NLRP3 inflammasome activation in vitro and in vivo, and NLRP3 deficiency in mice attenuated the decrease in body weight, grip strength, myocyte cross-sectional area, and restored the imbalance of protein synthesis and degradation in skeletal muscle induced by Ang II. In addition, we also demonstrated that mtROS/MtD mediated Ang II-induced NLRP3 inflammasome activation in skeletal muscle; and treatment with the mitochondrial targeted antioxidant, Mito-TEMPO, significantly inhibited mitochondrial reactive oxygen species (mtROS), MtD, NLRP3 inflammasome activation, and restored Ang II-induced skeletal muscle atrophy. Finally, we revealed the mechanisms linking PPAR-γ to the MtD/NLRP3 inflammasome in skeletal muscle. The PPAR-γ agonist protected against Ang II-induced muscle wasting by inhibiting the MtD/NLRP3 inflammasome pathway both in vitro and in vivo. Therefore, the PPAR-γ/MtD/NLRP3 inflammasome axis might

◀ **Fig. 5 The PPAR-γ antagonist T0070907 aggravated Ang II-induced muscle wasting by increasing mtROS/MtD and NLRP3 inflammasome activation in C2C12 myotubes.** Cells were pretreated with T0070907 (10 μM) for 1 h and then incubated with Ang II (10^{-6} mol/L) for 24 h. **a** Western blotting analysis of PPAR-γ, MyHC, p-Akt, Akt, p-PI3K, PI3K, p-mTOR, and mTOR in C2C12 myotubes. **b** Quantification of PPAR-γ, MyHC, the ratio of p-Akt to the Akt, p-PI3K to PI3K, and p-mTOR to mTOR expression normalized to β-actin. **c** The expression of Atrogin-1, MuRF-1, and myostatin in C2C12 myotubes was performed using real-time PCR. **d**, **e** The SOD2 activity and MDA level in C2C12 myotubes were determined according to the manufacturer's protocol. **f** Representative images of total ROS production by DCFDA staining and mitochondrial ROS by MitoSOX Red staining in C2C12 myotubes (scale bar: 50 μm, magnification: 200×). **g** Quantification of 2′,7′-dichlorofluorescein and MitoSOX Red fluorescence intensity. **h** Representative images of JC-1 staining in C2C12 myotubes. JC-1 aggregates (590 nm, red); JC-1 monomers (530 nm, green) (scale bar: 50 μm, magnification: 200×). **i** Quantification of JC-1 fluorescence intensity. **j** ATP production in C2C12 myotubes was determined according to the manufacturer's protocol. **k** & **l** The mtDNA copy number and *Mt-nd1* level in C2C12 myotubes normalized to *Gapdh* were detected using real-time PCR. **m** Western blotting analysis of NLRP3, caspase-1, ASC, IL-1β, and IL-18 in C2C12 myotubes. **n** Quantification of NLRP3, caspase-1, ASC, IL-1β, and IL-18 expression normalized to β-actin. The values represent the mean ± SD ($n = 6$). $^{*}P < 0.05$, compared with the control group; $^{**}P < 0.01$, compared with the control group. $^{\#}P < 0.05$, the Ang II + T0070907 group versus the Ang II group.

represent a therapeutic target to treat Ang II-induced skeletal muscle wasting.

Inflammasomes are multi-protein platforms that mediate the activation of caspases and induced inflammation. Among them, the NLRP3 inflammasome, a crucial regulator of innate immunity, is the best known. After formation and activation, the NLRP3 inflammasome associates with the adaptor protein apoptosis speck-like protein containing a caspase recruitment domain (ASC), which then induces the auto-catalytic cleavage and activation of procaspase-1. Activated caspase-1 cleaves pro-IL-1β and pro-IL-18 to their mature forms, generating the feedback mechanism that triggers the inflammatory response [23]. NLRP3 inflammasomes are active not only in immune cells, but also in non-immune cells, including myocytes and renal cells [24]. Our previous study demonstrated that NLRP3 inflammasomes were involved in aldosterone-induced renal tubular cell injury and unilateral ureteral obstruction (UUO)-induced renal fibrosis [25, 26]. To date, the NLRP3 inflammasome has been poorly studied in skeletal muscle [27, 28]. In the present study, we found that Ang II dose-dependently activated NLRP3 inflammasomes in C2C12 myotubes, and induced C2C12 myotube atrophy by the disruption of protein synthesis via inhibiting the PI3K/AKT/mTOR signaling pathway and the induction of protein degradation (such as Atrogin-1, MuRF-1, and myostatin). In addition, *Nlrp3* silencing significantly attenuated the Ang II-induced protein imbalance. In vivo, *Nlrp3* deletion markedly attenuated the body weight loss, gastrocnemius muscle mass loss, decreased grip strength, and reduced gastrocnemius cross-sectional areas that were observed in the Ang II-infused group. Furthermore, the Ang II-induced imbalance of proteins in the gastrocnemius muscle was reversed in *Nlrp3*$^{-/-}$ mice. These data strongly indicated the pathogenic role of the NLRP3 inflammasome in Ang II-mediated muscle wasting.

The potential mechanisms of Ang II-induced NLRP3 inflammasome activation were further investigated. Recent research suggested that the NLRP3 inflammasome could be activated by a wide range of danger signals, including ROS, Ca^{2+}, nitric oxide (NO), and MtD. Excessive ROS generation was identified as the most common pathway in NLRP3 inflammasome assembly, and treatment with ROS inhibitors could decrease NLRP3 inflammasome-dependent pyroptosis, which suggested that ROS served as direct activators of NLRP3 inflammasomes [29, 30]. The imbalance between increased ROS generation and limited antioxidant capacity could lead to severe damage to cellular function. Mitochondria are the major source of cellular ROS; however, they are also the main targets attacked by ROS. There is evidence that ROS production in mitochondria is crucial for MtD and decreased mitochondrial content [31]. Increasing evidence suggests that MtD contributes to skeletal muscle wasting [32]. In the present study, in cultured C2C12 myotubes, Ang II induced increased mitochondrial ROS (as determined by MitoSOX staining and DCFDA staining). However, the mitochondria-targeted antioxidant, Mito-TEMPO, significantly inhibited Ang II-induced ROS generation in vitro. Based on previous observations and our data, we hypothesized that the protective effect of Mito-TEMPO on C2C12 cell injury might be mediated, at least partly, through the mtROS/MtD pathway.

To further determine MtD in AngII-induced muscle wasting, we set up an in vitro experiment using C2C12 myotubes subjected to Ang II incubation. As expected, Ang II induced MtD, as evidenced by impaired △ψm, decreased mtDNA copy numbers, Mt-nd1 expression, and ATP content. Treatment with Mito-TEMPO dramatically reversed these mitochondrial abnormalities. Although MtD has been suggested to lead to skeletal muscle wasting, the relationship between mtROS/MtD and NLRP3 inflammasome activation in response to Ang II-induced muscle wasting was unclear. The present study showed that Mito-TEMPO robustly blocked Ang II-induced NLRP3 inflammasome activation and the imbalance of proteins in C2C12 myotubes, suggesting a pathogenic role for the mtROS/MtD/NLRP3 inflammasome axis in Ang II-induced skeletal muscle wasting. Recently, Wei et al. reported that Ang II markedly induced NADPH oxidase activation in skeletal muscle cells [33, 34]; Sukhanov et al. also indicated the involvement of dual oxidases (NADPH

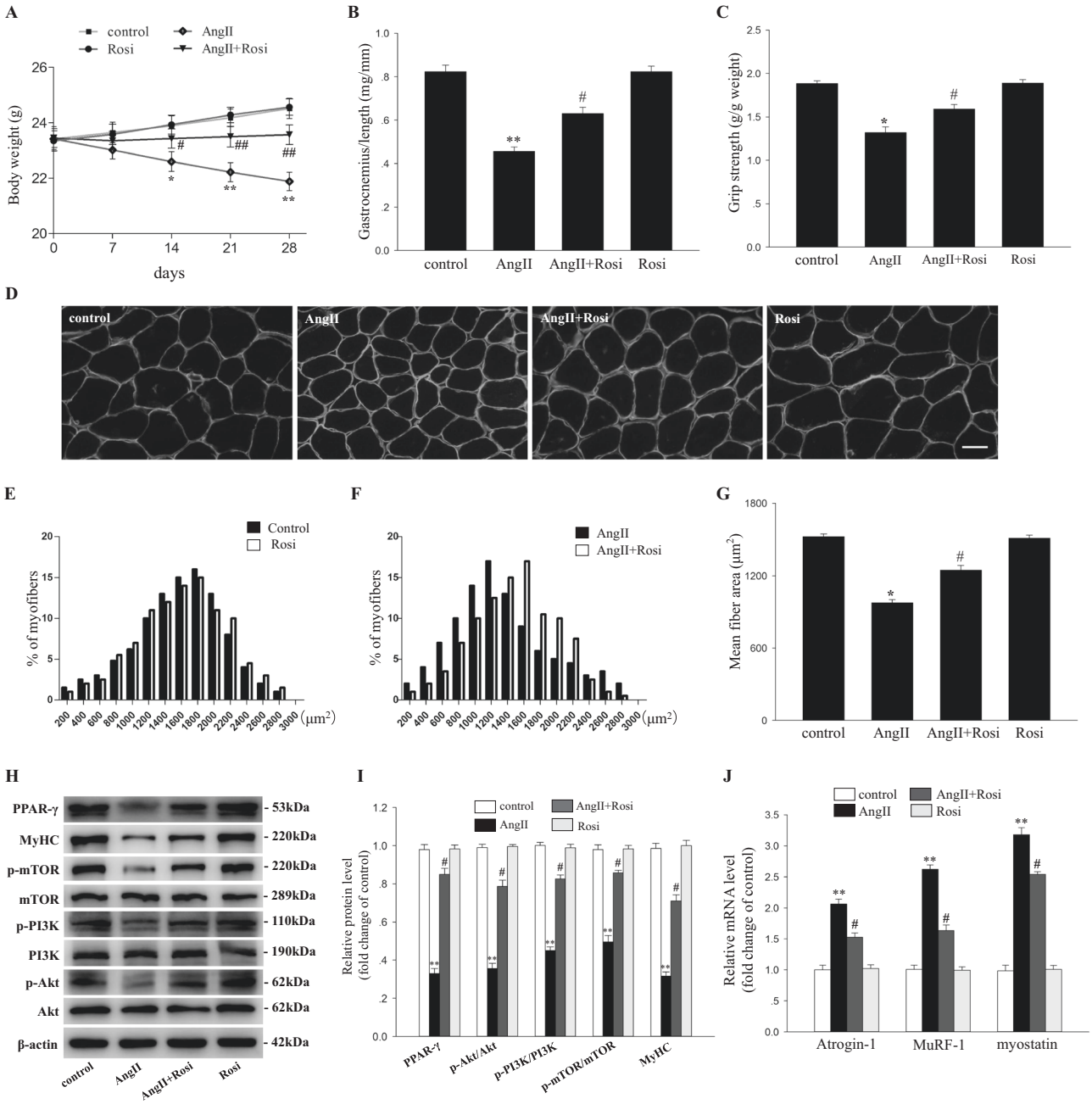

Fig. 6 The PPAR-γ agonist rosiglitazone attenuated Ang II-induced muscle wasting in vivo. a Body weight changes in the control mice and Ang II mice, with or without rosiglitazone. **b** Gastrocnemius muscle weight normalized to tibia length. (**c**) Measurement of muscle grip strength in the control mice and Ang II mice, with or without rosiglitazone. **d** Representative photomicrographs of gastrocnemius sections stained with dystrophin (scale bar: 20 μm, magnification: 400×). **e** & **f** Distribution of myofiber cross-sectional area (CSA) in gastrocnemius muscles of the control mice and Ang II mice, with or without rosiglitazone. **g** Mean myofiber area in gastrocnemius muscles. **h** Protein expressions of PPAR-γ, MyHC, p-Akt, Akt, p-PI3K, PI3K, p-mTOR, and mTOR in gastrocnemius muscles of different groups were determined by western blotting. **i** Quantification of PPAR-γ, MyHC, the ratio of p-Akt to the Akt, p-PI3K to PI3K, and p-mTOR to mTOR expression normalized to β-actin. **j** Real-time PCR was used to detect the expression of Atrogin-1, MuRF-1, and myostatin in gastrocnemius muscles of the control mice and Ang II mice, with or without rosiglitazone normalized to GAPDH. Results were presented as the mean ± SD ($n = 6$). $^{*}P < 0.05$, compared with the control group; $^{**}P < 0.01$, compared with the control group. $^{\#}P < 0.05$, the Ang II + Rosi group versus the Ang II group. Rosi, rosiglitazone.

oxidase and the MtD mitochondrial system) in Ang II-induced muscle wasting [12]. These results raised the question of mitochondrial/NADPH oxidase cross-talk in Ang II-induced ROS and muscle wasting. Daiber observed that Ang II activated NADPH oxidase, and subsequently, NADPH oxidase-dependent ROS attacked mitochondrial

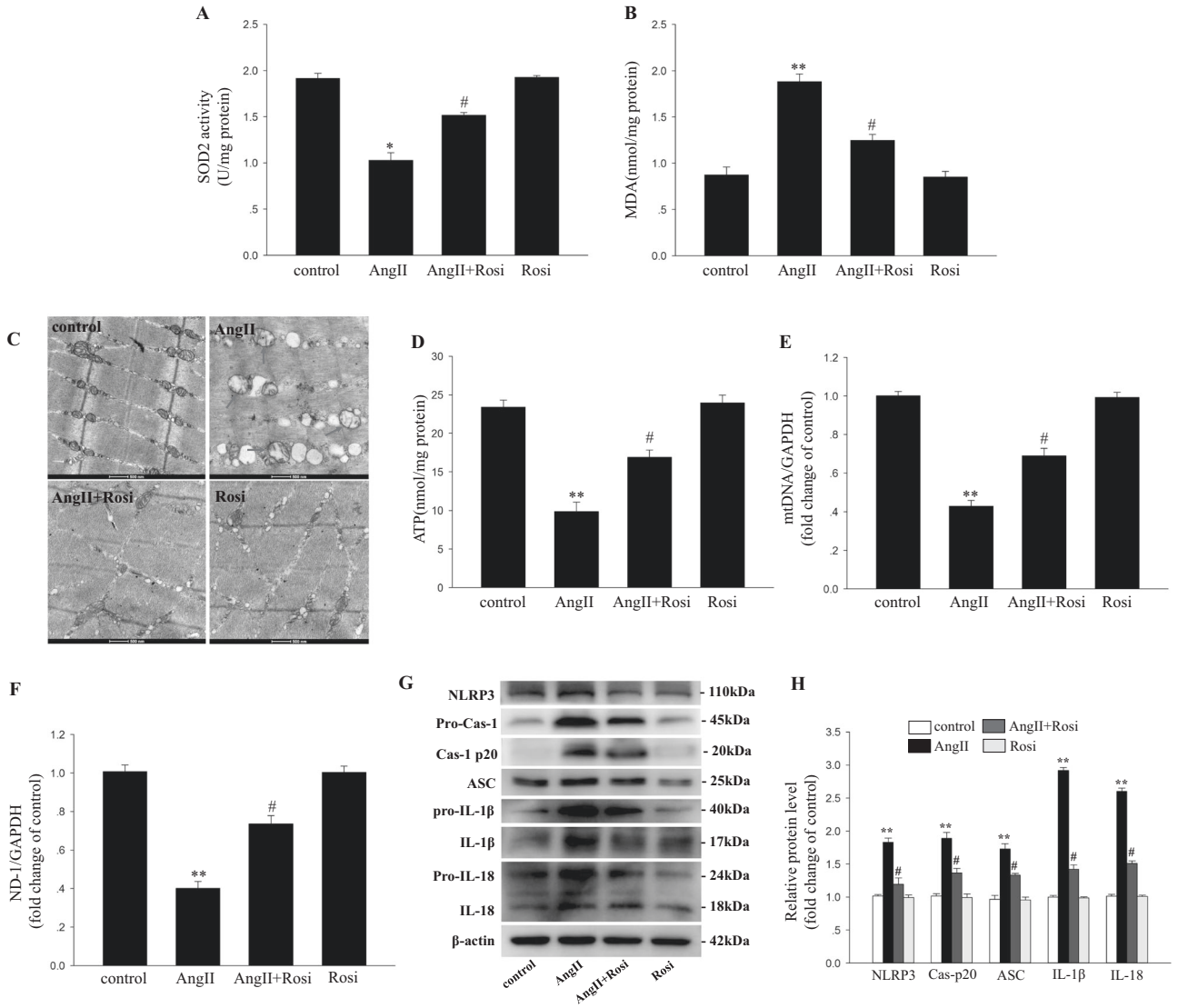

Fig. 7 The PPAR-γ agonist rosiglitazone ameliorated muscle wasting by suppressing MtD and the NLRP3 inflammasome in vivo. **a**, **b** The SOD2 activity and MDA level in gastrocnemius muscles were assessed according to the manufacturer's protocols. **c** Representative electron microscopy photomicrographs of the ultrastructural morphology of mitochondria in gastrocnemius muscles (scale bar: 500 nm, magnification: 10,000×). **d** ATP production in gastrocnemius muscles was evaluated according to the manufacturer's protocol. **e** & **f** The mRNA level of mtDNA and *Mt-nd1* normalized to *Gapdh* were determined using real-time PCR, respectively. **g** Western blot of NLRP3, caspase-1, ASC, IL-1β, and IL-18 in gastrocnemius muscles. **h** Quantification of NLRP3, caspase-1, ASC, IL-1β, and IL-18 expression normalized to β-actin. Results are presented as the mean ± SD ($n = 6$). *$P < 0.05$, compared with the control group; **$P < 0.01$, compared with the control group. #$P < 0.05$, the Ang II + Rosi group versus the Ang II group. Rosi, rosiglitazone.

ATP-sensitive potassium channels, leading to MtD and increased mtROS, which activated the NADPH oxidase cycle [35]. Further research into the mechanism of the cross-talk between NADPH oxidase and mitochondria in skeletal muscle wasting is required.

Finally, we provided direct evidence that PPAR-γ acts as a key regulator of the MtD/NLRP3 inflammasome axis in Ang II-induced skeletal muscle wasting. PPAR-γ is a ligand-activated transcription factor that belongs to the nuclear hormone receptor family. Although PPAR-γ was thought to regulate the metabolism of glucose and lipids, it also plays important roles in various physiological functions [15]. A previous study suggested that PPAR-γ agonists rescued the mitochondrial dyfunction caused by inhibition of complex I in neurodegenerative models [17]. Moreover, the PPAR-γ agonist rosiglitazone prevented Ang II-induced inflammation in vascular smooth muscle cells [36]. However, the metabolic functions of PPAR-γ in nonadipose tissue are not well understood, especially in skeletal muscle. To explore the molecular mechanism underlying the protective role of PPAR-γ on skeletal muscle function, we tested the response of the mtROS/MtD/NLRP3

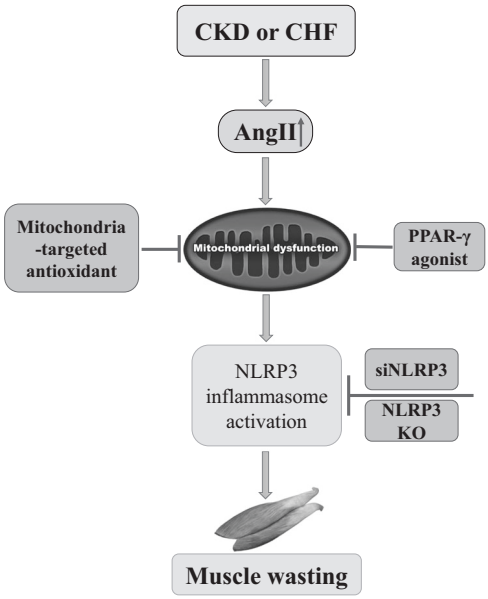

Fig. 8 Potential signaling pathways involved in Ang II-induced muscle wasting.

inflammasome axis to rosiglitazone. The results showed that rosiglitazone inhibited mtROS and MtD (characterized by impaired △ψm); decreased mtDNA copy numbers, Mt-nd1 expression, and the ATP content; and reduced NLRP3 inflammasome activation in C2C12 myotubes. Most importantly, rosiglitazone significantly ameliorated Ang II-induced disruption of protein synthesis and the induction of protein degradation. Next, we observed the role of the PPAR-γ inhibitor T0070907 in muscle wasting. T0070907 exacerbated Ang II-induced mtROS production, MtD, NLRP3 inflammasome activation, and protein imbalance. Based on these results, we suggested that pharmacological targeting of PPAR-γ/MtD/NLRP3 inflammasome signaling may represent a novel approach to treat muscle wasting. To further investigate this proposal, we assessed the role of rosiglitazone in Ang II-infused skeletal muscle wasting in vivo. Rosiglitazone attenuated the impaired skeletal function by increasing grip strength, the myocyte cross-sectional area, and reducing the imbalance of protein synthesis and the degradation of the gastrocnemius muscle. In addition, rosiglitazone also inhibited ROS generation, attenuated the impaired mitochondrial morphology and function, and NLRP3 inflammasome activation in the Ang II-induced model. Our findings partially revealed the mechanism of Ang II-induced muscle wasting and identified PPAR-γ as a pharmacological target to treat muscle wasting.

In conclusion, muscle wasting often occurs in patients with CKD and CHF, and increased Ang II is involved in the progression of these disease. Our data showed that the MtD/NLRP3 inflammasome axis mediates Ang II-induced muscle wasting. Thus, the use of siRNA or genetic depletion of NLRP3, pharmacological antioxidants, or PPAR-γ agonists significantly normalized muscle function and the protein energy balance (Fig. 8). The present study provided evidence of a novel downstream pathway in Ang II-induced skeletal muscle wasting and suggested that targeting the PPAR-γ/MtD/NLRP3 inflammasome axis might provide a therapeutic approach to treat Ang II-mediated muscle wasting.

Acknowledgements This work was sponsored by Shanghai Pujiang Program (17PJD021), the interdisciplinary program of Shanghai Jiao Tong University (YG2017MS07), the distinguished Young Scholar of Ninth People's Hospital (jyyq09201701), and the SHIPM-mu fund no. JC201805 from Shanghai Institute of Precision Medicine, Ninth People's Hospital Shanghai affiliated to Jiao Tong University School of Medicine.

Compliance with ethical standards

Conflict of interest The authors declare that they have no conflict of interest.

Publisher's note Springer Nature remains neutral with regard to jurisdictional claims in published maps and institutional affiliations.

References

1. Cohen S, Nathan JA, Goldberg AL. Muscle wasting in disease: molecular mechanisms and promising therapies. Nat Rev Drug Discov. 2015;14:58–74.
2. Yoshida T, Tabony AM, Galvez S, Galvez WE, Mitch Y, Higashi S, et al. Molecular mechanisms and signaling pathways of angiotensin II-induced muscle wasting: potential therapeutic targets for cardiac cachexia. Int J Biochem Cell Biol. 2013;45:2322–32.
3. Zhang L, Du J, Hu Z, Han G, Delafontaine P, Garcia G, et al. IL-6 and serum amyloid A synergy mediates angiotensin II-induced muscle wasting. J Am Soc Nephrol. 2009;20:604–12.
4. Brink M, Price SR, Chrast J, Bailey JL, Anwar A, Mitch WE, et al. Angiotensin II induces skeletal muscle wasting through enhanced protein degradation and down-regulates autocrine insulin-like growth factor. Endocrinology. 2001;142:1489–96.
5. Mitsuishi M, Miyashita K, Muraki A, Itoh H. Angiotensin II reduces mitochondrial content in skeletal muscle and affects glycemic control. Diabetes. 2009;58:710–7.
6. Yoshida T, Galvez S, Tiwari S, Rezk BM, Semprun-Prieto L, Higashi Y, et al. Angiotensin II inhibits satellite cell proliferation and prevents skeletal muscle regeneration. J Biol Chem. 2013;288:23823–32.
7. Costamagna D, Costelli P, Sampaolesi M, Penna F. Role of inflammation in muscle homeostasis and myogenesis. Mediators Inflamm. 2015;2015:805172.
8. Jatoi A, Dakhil SR, Nguyen PL, Sloan JA, Kugler JW, Rowland KJ, et al. A placebo-controlled double blind trial of etanercept for the cancer anorexia/weight loss syndrome: results from N00C1 from the North Central Cancer Treatment Group. Cancer. 2007;110:1396–403.
9. Jatoi A, Ritter HL, Dueck A, Nguyen PL, Nikcevich DA, Luyun RF, et al. A placebo-controlled, double-blind trial of infliximab for

cancer-associated weight loss in elderly and/or poor performance non-small cell lung cancer patients (N01C9). Lung Cancer. 2010;68:234–9.
10. Bayliss TJ, Smith JT, Schuster M, Dragnev KH, Rigas JR. A humanized anti-IL-6 antibody (ALD518) in non-small cell lung cancer. Expert Opin Biol Ther. 2011;11:1663–8.
11. Apel K, Hirt H. Reactive oxygen species: metabolism, oxidative stress, and signal transduction. Annu Rev Plant Biol. 2004;55: 373–99.
12. Sukhanov S, Semprun-Prieto L, Yoshida T, Michael TA, Higashi Y, Galvez S, et al. Angiotensin II, oxidative stress and skeletal muscle wasting. Am J Med Sci. 2011;342:143–7.
13. Argiles JM, Lopez-Soriano FJ, Busquets S. Muscle wasting in cancer: the role of mitochondria. Curr Opin Clin Nutr Metab Care. 2015;18:221–5.
14. Tabony AM, Yoshida T, Sukhanov S, Delafontaine P. Protein phosphatase 2C-alpha knockdown reduces angiotensin II-mediated skeletal muscle wasting via restoration of mitochondrial recycling and function. Skelet Muscle. 2014;4:20.
15. Grygiel-Gorniak B. Peroxisome proliferator-activated receptors and their ligands: nutritional and clinical implications-a review. Nutr J. 2014;13:17.
16. Håkansson J, Eliasson B, Smith U, Enerback S. Adipocyte mitochondrial genes and the forkhead factor FOXC2 are decreased in type 2 diabetes patients and normalized in response to rosiglitazone. Diabetol Metab Syndr. 2011;3:32.
17. Corona JC, de Souza SC, Duchen MR. PPARgamma activation rescues mitochondrial function from inhibition of complex I and loss of PINK1. Exp Neurol. 2014;253:16–27.
18. Carta AR. PPAR-gamma: therapeutic prospects in Parkinson's disease. Curr Drug Targets. 2013;14:743–51.
19. Fogo AB. PPARgamma and chronic kidney disease. Pediatr Nephrol. 2011;26:347–51.
20. Bing C, Russell S, Becket E, Pope M, Tisdale MJ, Trayhurn P, et al. Adipose atrophy in cancer cachexia: morphologic and molecular analysis of adipose tissue in tumour-bearing mice. Br J Cancer. 2006;95:1028–37.
21. Beluzi M, Peres SB, Henriques FS, Sertie RA, Franco FO, Santos KB, et al. Pioglitazone treatment increases survival and prevents body weight loss in tumor-bearing animals: possible anti-cachectic effect. PLoS ONE. 2015;10:e122660.
22. Takeshita H, Yamamoto K, Nozato S, Inagaki T, Tsuchimochi H, Shirai M, et al. Modified forelimb grip strength test detects aging-associated physiological decline in skeletal muscle function in male mice. Sci Rep. 2017;7:42323.
23. Artlett CM, Thacker JD. Molecular activation of the NLRP3 Inflammasome in fibrosis: common threads linking divergent fibrogenic diseases. Antioxid Redox Signal. 2015;22:1162–75.
24. Bracey NA, Beck PL, Muruve DA, Hirota SA, Guo J, Jabagi H, et al. The Nlrp3 inflammasome promotes myocardial dysfunction in structural cardiomyopathy through interleukin-1beta. Exp Physiol. 2013;98:462–72.
25. Ding W, Guo H, Xu C, Wang B, Zhang M, Ding F. Mitochondrial reactive oxygen species-mediated NLRP3 inflammasome activation contributes to aldosterone-induced renal tubular cells injury. Oncotarget. 2016;7:17479–91.
26. Guo H, Bi X, Zhou P, Zhu S, Ding W. NLRP3 deficiency attenuates renal fibrosis and ameliorates mitochondrial dysfunction in a mouse unilateral ureteral obstruction model of chronic kidney disease. Mediators Inflamm. 2017; 2017:8316560.
27. Boursereau R, Abou-Samra M, Lecompte S, Noel L, Brichard SM. Downregulation of the NLRP3 inflammasome by adiponectin rescues Duchenne muscular dystrophy. BMC Biol. 2018;16:33.
28. McBride MJ, Foley KP, D'Souza DM, Li YE, Lau TC, Hawke TJ, et al. The NLRP3 inflammasome contributes to sarcopenia and lower muscle glycolytic potential in old mice. Am J Physiol Endocrinol Metab. 2017;313:E222–E232.
29. Sun HJ, Ren XS, Xiong XQ, Chen YZ, Zhao MX, Wang JJ, et al. NLRP3 inflammasome activation contributes to VSMC phenotypic transformation and proliferation in hypertension. Cell Death Dis. 2017;8:e3074.
30. Dostert C, Pétrilli V, Van Bruggen R, Steele C, Mossman BT, Tschopp J. Innate immune activation through Nalp3 inflammasome sensing of asbestos and silica. Science. 2008;320:674–7.
31. Liu J, Peng Y, Feng Z, Shi W, Qu L, Li Y, et al. Reloading functionally ameliorates disuse-induced muscle atrophy by reversing mitochondrial dysfunction, and similar benefits are gained by administering a combination of mitochondrial nutrients. Free Radic Biol Med. 2014;69:116–28.
32. Cheng Y, Di S, Fan C, Cai L, Gao C, Jiang P, et al. SIRT1 activation by pterostilbene attenuates the skeletal muscle oxidative stress injury and mitochondrial dysfunction induced by ischemia reperfusion injury. Apoptosis. 2016;21:905–16.
33. Wei Y, Sowers JR, Nistala R, Gong H, Uptergrove GM, Clark SE, et al. Angiotensin II-induced NADPH oxidase activation impairs insulin signaling in skeletal muscle cells. J Biol Chem. 2006;281:35137–46.
34. Javeshghani D, Magder SA, Barreiro E, Quinn MT, Hussain SN. Molecular characterization of a superoxide-generating NAD(P)H oxidase in the ventilatory muscles. Am J Respir Crit Care Med. 2002;165:412–8.
35. Daiber A. Redox signaling (cross-talk) from and to mitochondria involves mitochondrial pores and reactive oxygen species. Biochim Biophys Acta. 2010;1797:897–906.
36. Ji Y, Liu J, Wang Z, Liu N, Gou W. PPARgamma agonist, rosiglitazone, regulates angiotensin II-induced vascular inflammation through the TLR4-dependent signaling pathway. Lab Invest. 2009;89:887–902.